Variation of the coastline in a medium period (1972-2020): An analysis in the municipality of Soure, *paraense* Amazon

Variação da linha costeira em um médio período (1972-2020): uma análise no município de Soure, Amazônia paraense

Rafael Alexandre Alves Menezes[I] | Diandra Karina Martins Guimarães[I] | Maamar El Robrini[I]

[I]Universidade Federal do Pará. Belém, Pará, Brazil

Abstract: Estuarine erosion is a significant environmental issue that affects various coastal regions around the world. The western coast of the Pará River estuary mouth is located in the municipality of Soure, in the state of Pará. To analyze the multitemporal variability of erosive and/or accretion rates of the coastline (CL), remote sensing techniques and the Digital Shoreline Analysis System (DSAS) were employed. Based on orbital imagery from the Landsat sensors (MSS, TM, OLI) from 1972 to 2020, the CL for each year was detected using the Modified Normalized Difference Water Index (MNDWI). This approach enabled the creation of transects from the onshore baseline and the quantification of NSM, EPR, and LRR rates, processed using DSAS v5. The results indicated that erosion is predominant in 57% of the transects, while accretion was observed in 43%, with an average erosion rate of –2.1 m/year (Sector I–SE) and an average accretion rate of 2.55 m/year (Sector II–NE). The results obtained through remote sensing techniques generated substantial data on the dynamics of the CL, corroborating essential technical procedures for implementing mitigation measures in the region and in other geographical areas.

Keywords: DSAS v5. Estuarine dynamics. Erosion. GIS. Remote sensing.

Resumo: A erosão estuarina é um problema ambiental significativo que afeta várias regiões costeiras ao redor do mundo. A costa oeste da foz do estuário do rio Pará se localiza no município de Soure, no Pará. Para analisar a variabilidade multitemporal das taxas erosivas e/ou a acreção da linha costeira (LC), foi utilizado o sensoriamento remoto e o *Digital Shoreline Analysis System* (DSAS). A partir de imagens orbitais dos sensores Landsat (MSS, TM, OLI) de 1972 a 2020, a LC de cada ano foi detectada utilizando o índice da diferença de água normalizada modificado (MNDWI). Essa abordagem permitiu a criação de transectos a partir da linha de base *onshore*, e a quantificação das taxas de NSM, EPR e LRR, processadas via DSAS v5. Os resultados mostraram que a erosão é predominante em 57% dos transectos, enquanto a acreção foi detectada em 43% dos transectos, sendo que a taxa média de erosão foi de -2,1 m/ano (setor I-SE) e a taxa média de acreção foi de 2,55 m/ano (setor II-NE). Os resultados obtidos através das técnicas de sensoriamento remoto geraram dados substanciais sobre a dinâmica da LC, corroborando procedimentos técnicos essenciais para implementar medidas de mitigação na região e em outros espaços geográficos.

Palavras-chave: DSAS v5. Dinâmica estuarina. Erosão. GIS. Sensoriamento remoto.

Menezes, R. A. A., Guimarães, D. K. M., & El Robrini, M. (2025). Variation of the coastline in a medium period (1972-2020): An analysis in the municipality of Soure, *Paraense* Amazon. *Boletim do Museu Paraense Emílio Goeldi. Ciências Naturais*, *20*(3), e2025-1020. http://doi.org/10.46357/bcnaturais.v20i3.1020

Corresponding author: Rafael Alexandre Alves Menezes. Rua Augusto Corrêa, 1 - Guamá. Belém, PA, Brazil. CEP 66075-110 (rafa.menezes1996@gmail.com).

Received on 08/22/2024
Approved on 11/25/2025
Editorial responsibility: Milena Marília Nogueira de Andrade

INTRODUCTION

The Coastal Zone (CZ) refers to the geographic area of interaction between the air, sea, and land, including its renewable and non-renewable resources, encompassing both a maritime and a terrestrial strip (Baral et al., 2018). The former refers to the area extending twelve nautical miles from the baseline (low-water line), thus encompassing the entirety of the territorial sea. The latter is the area within the boundaries of municipalities affected by urbanization, port activities, tourism, and industrial activities (MMA, 2018).

The coastline (CL) is used as a geomorphological indicator of coastal dynamics due to its position being variable in time and space (Bertacchini, 2010; Jana et al., 2014; Mahapatra et al., 2014b; Ding et al., 2019). Its movement inland reflects retreat or erosion (Baral et al., 2018). Conversely, its movement towards the offshore or the bay represents advance or accretion (Silva et al., 2016). These changes occur over a medium (~100 years) period and can be characterized mainly through the analysis of data available from orbital sensors (França, 2003). The main factors acting on the CZ are: rainfall, winds, waves, tidal currents, sediment transport and deposition, leading to constant modifications of the CL (Kannan et al., 2014; Wang et al., 2014; Ahmed et al., 2021).

Remote sensing through CL detection technologies is frequently used to provide information about the morphology of the CZ. Thus, the mosaic of satellite images and the vectorization of the CL emerge as a way to identify variations occurring in the CZ (França, 2003; Genz et al., 2007; S. Rodrigues & Souza Filho, 2011; Mahapatra et al., 2014a; Luijendijk et al., 2018; Mentaschi et al., 2018; Orlando et al., 2019; Muskananfola et al., 2020). For the evaluation and quantification of erosion and accretion rates, the Digital Shoreline Analysis System (DSAS) applied to ArcGIS software (Starting from the ArcView GIS 3.x version) assists in determining the variations occurring in the CL over time and space, and is frequently used by the scientific community to analyze the dynamic fluctuations occurring on coasts worldwide (Farias & Maia, 2010; Conti & M. Rodrigues, 2011; Ranieri & El-Robrini, 2015; Mahapatra et al., 2014a; Himmelstoss et al., 2018; Galvez et al., 2020; C. A. G. Santos et al., 2021b).

The dynamics of the CL necessitate the identification and study of different aspects over various temporal perspectives, encompassing short, medium, and long-term spatialization (Tran Thi et al., 2014; Bheeroo et al., 2016; Chenthamil Selvan et al., 2016; Baral et al., 2018). For this purpose, the acquisition of satellite images and the utilization of Geographic Information System (GIS) environments provide a way to understand the dynamics of the LC over time. This includes data that can be found in numerous databases, allowing for the analysis of a large portion of space with satisfactory precision for the analysis component. Consequently, residual errors are minimized, resembling in situ approaches (Alesheikh et al., 2007; Al-Hatrushi, 2013; Esmail et al., 2019; C. A. G. Santos et al., 2021b).

Furthermore, the study of coastal geomorphology has an improvement configuration for the current scenario, a fact that is linked to the use of GIS (Mcfadden et al., 2007; Kaliraj et al., 2015; Li et al., 2015) and the use of the range of satellite images available from the United States Geological Survey (USGS) (França & Souza Filho, 2003; Mahapatra et al., 2014a; Souza Filho, 2005; Santos, 2017). The multitemporal variability of CL erosion or advance rates can be quantified using geospatial techniques, and the analysis of these data is used to understand the dynamics of the CZ, quantifying the rates of variables over time and space (Himmelstoss et al., 2018; Stanchev et al., 2018; Esmail et al., 2019; Nassar et al., 2019; Muskananfola et al., 2020; L. Lima et al., 2021; Mishra et al., 2022; Quadrado et al., 2021).

Many studies in the Brazilian CZ have been published in recent years on coastal analysis, each with its own temporal/spatial particularities and distinct variabilities (Silva et al., 2016; Duarte et al., 2018; Aquino da Silva et al., 2019; Carvalho et al., 2020). However, there are few studies focusing on LC dynamics in the Amazon, particularly in the state of Pará (Ranieri & El-Robrini, 2015; Baía et al., 2021).

Therefore, the study conceived from LC analysis, using satellite images from different years (through overlaying visually interpreted vectors) as the main method to identify variations in the Pará CZ (França, 2003; S. Rodrigues & Souza Filho, 2011). In this perspective, besides direct vector overlay and segmentation, the DSAS tool in ArcGIS software contributed to understanding the multitemporal variations occurring in the coastal scenario of Pará (Conti & M. Rodrigues, 2011; Ranieri & El-Robrini, 2015; Baía et al., 2021).

CZ of the largest fluvial-marine island on the planet (Marajó Island, Pará) is influenced by two major estuaries, those of the Amazon and Pará rivers. These are subject to constant morphological changes, imparting to the coast a dynamic due to its geographical position. The study area is in the eastern part of Marajó Island (Pará, 2020), influenced by the waters of the Pará River estuary, with physical processes at micro and mesoscale generated by forcings from different sources (astronomical tides and river discharge) (Prestes, 2016; Prestes et al., 2014, 2017, 2020). This shoreline comprises the mangrove belt known as the Macromare Mangrove Coast of the Amazon (CMMA), spanning 650 km along the coast from Marajó Bay (Pará) to Tubarão Point (Maranhão) (Souza Filho, 2005), forming part of the largest continuous mangrove belt on the planet, underscoring the importance of understanding coastal processes in the region.

Determining the multitemporal behavior of the CL systematically contributes to integrated coastal management (Pessoa et al., 2019). However, evaluating the evolutionary scenarios of the CZ becomes challenging, as they are subjected to hydrodynamic forces (waves, tides, sea level oscillation), neotectonics, climate (winds, rainfall), and anthropogenic factors (civil and private constructions, deforestation) (Boye et al., 2018; Ataol et al., 2019; Mishra et al., 2022; Ahmed et al., 2021; C. A. G. Santos et al., 2021a), which condition the geographical space of analysis with difficult-to-measure particularities. In some cases, natural dynamic vectors modify the CZ to extents unimaginable when compared to anthropogenic modifications. In this context, the study area corresponds to the western portion of the Pará River estuary (eastern shore of the municipality of Soure, Pará), where natural dynamism prevails, while anthropogenic influences are concentrated in the southeastern fragment of Soure municipality.

Based on the above, this manuscript aims to analyze the evolution of the CL in the western portion of the Pará River Estuary mouth from 1972 to 2020 (constrained by the available Landsat historical series), utilizing satellite imagery, geoprocessing techniques, and leveraging the DSAS v5 plugin to quantify and analyze changes over the proposed 48-year temporal scenario. Thus, the study seeks to comprehend erosive and accretionary dynamics occurring at this temporal scale and to examine the hydrographic aspects influencing the CL. This study focuses on a specific scenario compared to other CZs worldwide, prominently situated in the Brazilian Amazon, characterized by unique processes due to its geographical location and structural morphogenesis (hydrology, climate, geology, and geomorphology).

The generated results are of paramount importance for understanding estuarine dynamics and are expected to contribute to capacity development activities that can provide responses to policymakers and the local, national, and global society. The techniques and data measurements used can be reproduced comprehensively and coherently. Furthermore, this work aims to contribute to the studies in the Decade (2020-2030) of Ocean Science, particularly to United Nations Sustainable Development Goal 13, aiming to contribute to the reduction/mitigation of global changes.

MATERIALS AND METHODS

STUDY AREA

The study area encompasses the CL of the municipality of Soure, located in the mesoregion of Marajó (microregion of Arari), bounded by: NW: 0° 14' 3.23" S and 48° 59' 39.65" W; NE: 0° 14' 59.18" S and 48° 22' 0.99" W; SW: 0° 41' 58.61" S and 48° 59' 10.02" W; SE: 0° 51' 29.08" S and 48° 22' 16.88" W (Figure 1).

Figure 1. Location map of the Municipality of Soure, Marajó Island, 2024. Source: IBGE (2021), USGS (2018), ANA (2021).

This area belongs to the geomorphological unit of the Marajoara Gulf, characterized by estuarine and deltaic elements, forming an extensive Quaternary sedimentary basin with kilometric thickness, controlled by strike-slip faults that guide the mouth of the Amazon River. This unit is subdivided into two other geomorphological units: Fluvio-marine Plains and Low Amazon River Plateaus, which encompass a range of depositional environments of fluvial, marine, lacustrine, or mixed origin (Melo & Simões, 2016). On the eastern shore, the structure corresponding to Barreiras sediments is composed of sandstones and claystones, followed by Post-Barreiras sediments (Rossetti et al., 2008a, 2008b) (Figure 2).

Soure is climate is hot and humid, characterized by its proximity to the Atlantic Ocean, influenced by maritime conditions and its location near the equator, resulting in abundant solar energy. From December to May, Soure experiences the rainy season due to the influence of both the warm Atlantic Equatorial and Continental air masses, occasionally intersected by cold Atlantic polar air masses, which enhance precipitation. From June to November, the region experiences the dry season, with higher temperatures. The average annual temperature ranges between 24 °C and 32 °C (INMET, n.d.).

The winds in Soure reach speeds between 6.2 m/s and 7 m/s (INMET, n.d.), predominantly from the northeast direction due to the movement of the Intertropical Convergence Zone (ITCZ). Wind speeds can vary in intensity between the western and eastern sectors due to topographical differences. Vegetation cover

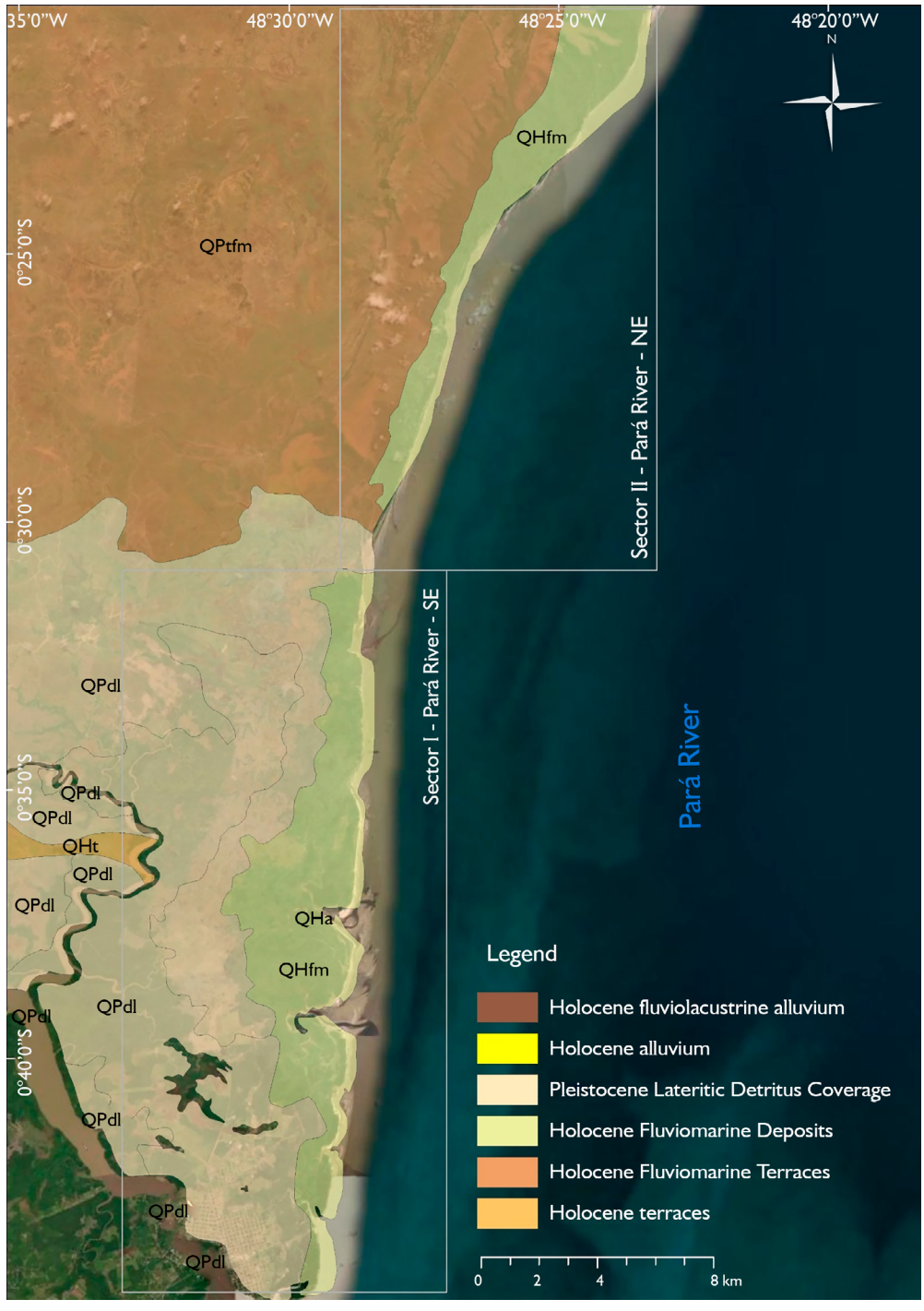

Figure 2. Geological map of the eastern shore of Marajó Island, 2024. Legends: QHfm = Holocene fluviomarine deposits, QPtfm = Pleistocene fluviomarine terraces, QPdl = Pleistocene lateritic detritus cover, QHt = Holocene terraces, QHa = Holocene alluvium. Source: Lacerda et al. (2008).

also influences wind patterns, as forests in the CZ act as natural barriers to winds coming from the northeast toward the eastern coast, significantly reducing their speed (A. Lima et al., 2005).

The eastern coast of Soure is influenced by the hydrodynamics of the Pará River, experiencing a meso to macrotidal regime (França & Souza Filho, 2003). The river flow rates are 98,594 m^3/s during the rainy season and 65,269 m^3/s during the dry season (El-Robrini et al., 2018). Tidal heights range from 5.6 m (high tide/spring tide) to 0.4 m (low tide/neap tide) (Marinha do Brasil, n.d.), and tidal currents reach speeds of 1.2 m/s (flood tide) and 1.4 m/s (ebb tide) (Rosário et al., 2016).

METHODOLOGY

The methodological procedure used to assess coastal erosion in Soure municipality, Pará, involved geospatial techniques in an office setting, utilizing data obtained from the Digital Shoreline Analysis System (DSAS) version 5 tool. The workflow is illustrated in Figure 3.

The process of selecting the projection system used in this study involves the prerequisite of quantifying the data to be generated and utilizing cartographic bases in reference systems with Universal Transverse Mercator (UTM) projections. Therefore, the chosen projection system uses meters (m) as the unit of measurement to calculate distances and project the position of specific components, providing quantitative data relevant to

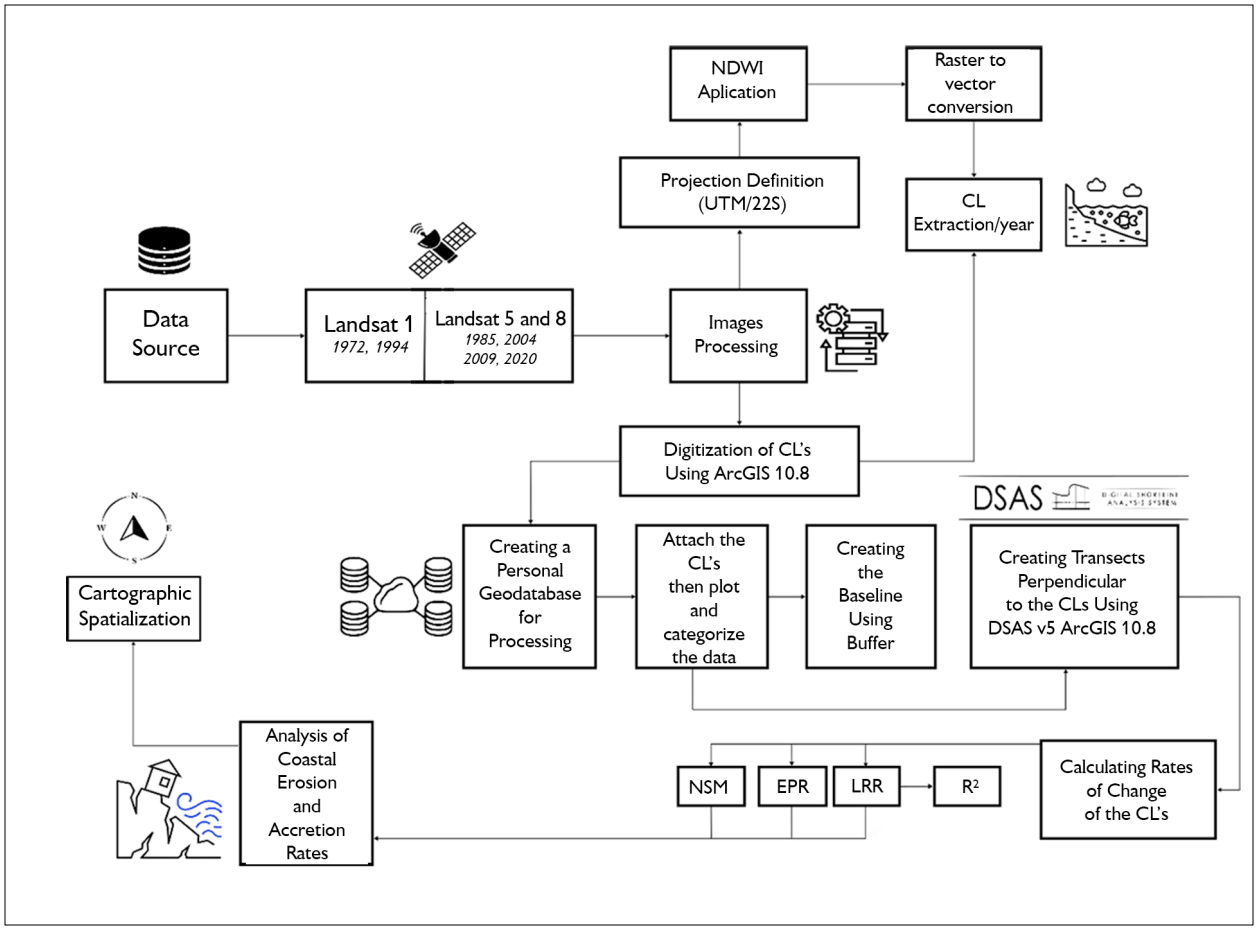

Figure 3. Methodological flow of coastal erosion analysis using DSAS v5. Organization: Author (2024).

the area in question. Additionally, the DSAS v5 plugin, employed in ArcGIS 10.8 software (accessed at the Geographic Information Lab - LAIG/UFPA), is based on the use of UTM coordinate system for interpolation within the GIS environment and quantification of data generated post-processing. If another type of projection were used, it would result in processing errors and prevent the generation of final data. Due to the area's large extent (~60 km), the study area is divided into two sectors: I) Rio Pará - SE and II) Rio Pará – NE (Figure 2).

ACQUISITION OF ORBITAL IMAGES

To ensure the execution of the analysis of CL variation in the areas influenced by the Pará River estuary, images were selected for comparison. These include Landsat 1 MSS medium-resolution images from 1972 and 1994, Landsat 5 TM images from 1985, 2004, and 2009 with a spatial resolution of 30 m, and Landsat 8 OLI images from 2020 with a spatial resolution of 15 m after merging band 8 (panchromatic). These images were obtained from the United States Geological Survey (USGS) website, accessed in September 2020 (Table 1). The selection of these image datasets was based on their minimal cloud cover (< 30%) over the coastal CL vectorization area.

CALCULATION OF GEOMETRIC ERRORS IN THE IMAGES

To ensure data reliability and result accuracy, a cumulative geometric error was defined among the images used. Considering the georeferencing error of each image extracted from the metadata and relating it proportionally to the pixel value, an error of 56.688 m was obtained, averaging 9,478 m annually for linear measurements and an error of 1,704.6 m^2, with 284.1 m^2 for polygonal area measurements (Table 2).

The calculated errors serve as control parameters for measuring the generated data, with the main focus on

Table 1. Satellite images and optical sensors used in processing. Source: USGS (2018). Organization: Author (2024).

Satellite	Optical sensor	Orbit point	Acquisition date	Climatic parameter	Hour	Spatial resolution (m)
Landsat 1	MSS	240060	13/12/1972	El Niño	12:56	80
Landsat 5	TM	224060	09/10/1985	No ocurrence	12:57	30
Landsat 1	MSS	224060	30/07/1994	No ocurrence	12:46	30
Landsat 5	TM	224060	23/06/2004	No ocurrence	13:10	30
Landsat 5	TM	224060	09/09/2009	El Niño	13:18	30
Landsat 8	OLI	224060	07/09/2020	La Niña	13:29	15

Table 2. Geometric errors in the images. Organization: Author (2024).

Year of image acquisition	Pixel error	Linear geometric error (m)
1972	0.370	11,124
1985	0.326	9,781
1994	0.384	11,523
2004	0.310	9,304
2009	0.352	10,573
2020	0.152	4,563
Accumulative geometric errors		56,868
Average errors		9,478

correlating them with the Coastal Net Shore Movement (NSM) data.

VECTORIZATION OF THE CL

The vectorization of CL was created using semi-automatic methods combined with manual methods, as proposed by Santos et al. (2021a). To compose the CL vector, spectral band calculations from Landsat and CL extraction in ArcMap 10.8 software were employed, converting raster (.tiff) features into lines (.shp). In detail, Near Infrared/Shortwave Infrared and Visible wavelength bands from Landsat sensors were utilized to differentiate land and water surfaces along the Coastal Zone (CZ). The infrared wavelength band was preferred because it aids in distinguishing water and land characteristics, where medium infrared energy is absorbed by water (or turbid water) and vegetation, while sand and other coastal features exhibit strong reflectance characteristics in this band (Alesheikh et al., 2007; C. A. G. Santos et al., 2021b).

In this composition, the Normalized Difference Water Index (NDWI) was used because it yielded more satisfactory results than other methods (e.g., visual interpretation of CL) and employs technically enhanced content for LC detection (Mishra et al., 2019; C. A. G. Santos et al., 2021b). The calculation of the Normalized Difference Water Index (NDWI) is

$$NDWeu = \frac{GREEN - NeuRG}{GREEN + NeuR}$$

Therefore, NDWI was applied to Landsat images in ArcMap 10.8, following the creation of a TIFF image with the NDWI component for each acquired Landsat image. Finally, it was vectorized to create the outline of CL in shapefile format.

DIGITAL SHORELINE ANALYSIS SYSTEM (DSAS)

All these data were generated using DSAS v5. To perform the calculations, DSAS requires three vector files: 1) the baseline, drawn parallel to the CL either onshore or offshore, i.e., within or outside the mainland, serving as the basis for CL movement calculations; 2) the transects, lines perpendicular to the coast responsible for calculating variations at specific points, segmenting the coastline from the baseline and crossing all available shorelines, automatically generated by DSAS, requiring only the assignment of interval between each transect; and 3) coastline vectors, each assigned to a date within the analyzed temporal range (Honeycutt et al., 2001).

122 transects were drawn perpendicular to the CL with a spacing of 100 meters between them due to the length of the analyzed coastline (~50 km). The settings establish a baseline, located inland relative to the oldest CL (1972), which serves as the starting point for measurements across all generated CL's.

The most commonly used methods for analyzing CL through DSAS are Coastal Net Shore Movement (NSM), End Point Rate (EPR), and Linear Regression Rate (LRR). Therefore, EPR is widely employed on the coast of the United States of America as it uses only two positions of the shoreline to calculate the rates of variation over time (Dolan et al., 1991).

LRR has shown satisfactory results, as demonstrated in the study by Honeycutt et al. (2001), where it was used to calculate long-term erosion rates and predict subsequent positions with a reduction in error of over 70% in New York and 34% in Delaware, including storm-prone coastal areas. Thus, the EPR and LRR analysis components have been highly successful in analyzing CL variation and are consequently the most widely used methods in the scientific field for coastal studies with DSAS (Honeycutt et al., 2001).

NSM measures the distance between the oldest and newest shorelines for each transect. Positive values indicate seaward movement, while negative values indicate landward movement of the CL (Himmelstoss et al., 2018; Kabir et al., 2020).

This article employs the NSM, EPR, and LRR methods, widely accepted in the scientific community (Nascimento, 2012; Mahapatra et al., 2014a; Misra & Balaji, 2015;

Almonacid-Caballer et al., 2016; Kabir et al., 2020; Muskananfola et al., 2020; C. A. G. Santos et al., 2021b), yielding satisfactory results. The rationale for using these methods lies in their ability to accurately calculate CL variation rates and identify medium-term behavioral trends through the coefficient of determination (R^2), where the calculation is:

$$R^2 = 1 - \sqrt{\frac{\sum(y - y')^2}{\sum(y - \bar{y})}}$$

Where,

R^2 is the coefficient of determination;

y is the measured distance from the baseline to a CL data point;

y' is the predicted distance from the baseline based on the equation of the best-fit regression line; and

$\bar{y}$ is the mean of the measured distances of CL from the baseline.

In this sense, R^2 or the Coefficient of Determination, indicates a close relationship between the generated and analyzed data. A value of R^2 close to 1 signifies a satisfactory correlational trend in the data. This suggests a perspective of continuity in the ongoing process (accretion). Conversely, if R^2 is close to 0, it indicates an unsatisfactory correlation among the analyzed data. In such cases, it suggests a perspective of stagnation or discontinuity (erosion) in the current coastal conditioning process (Allan et al., 2003; Maiti & Bhattacharya, 2009; Himmelstoss et al., 2018).

RESULTS

The multi-temporal variability of CL constitutes a scalar-temporal parameter spanning a medium period (1972-2020) in the CZ of the municipality of Soure (~50 km) (Tables 3 and 4). Following the application of DSAS v5, 282 transects were obtained to measure CL changes (Figure 4). Erosion was observed in 160 transects, while accretion was detected in 122 transects (Figure 4; Table 3). Thus, at the mouth of the Pará River estuary, between 1972 and 2020, CL experienced erosion in 57% of transects and accretion in 43%.

The results showed that the maximum erosion distance was -1,247.46 m, while the maximum accretion distance was 1,012.72 m, observed on the southeast (SE) shore of Soure. The findings indicate certain regions with maximum erosion rates, notably the SE coast (-29.41 m/year) (Figure 4; Tables 3 and 4).

The dynamic complexity of the study object needs to be understood in segmented sections. Given that there are dynamic processes acting on the analyzed coastline differently, the following subtopics are necessary to address and focus on the results more directly.

SECTOR I – PARÁ RIVER – SE

Sector I (~27 km) comprises a set of 160 transects (497-656). Statistical modeling quantification reveals a predominant erosive trend. Accordingly, 46 transects (29%) showed accretion tendencies, while 114 transects (71%) exhibited erosive characteristics, with an average coastline retreat rate of -2.1 m/year (Figure 4).

The parameter $R^2 > 0.5$ includes 87 transects, whereas 73 transects with $R < 0.5$ were identified, comprising 54% and 46% for their respective segments. These data indicate a perspective of ongoing processes in the CZ. In this scenario, there is an alternation of dynamic processes; according to R^2 statistics, sedimentation predominates. However, intense erosion is also identified in the quantified data (Table 3).

NSM results indicate an erosive trend of the CL. The average rate from this method is -113.81 m. The highest erosion rate recorded was -1,247.46 m (transect 586), with an average of -193.5 m. Conversely, the advancement of the CL shows a rate of 1,012.72 m (transect 583), with an average rate lower than that of erosion, at 110.07 m (Figures 4 and 5A, Table 4).

The retreat of the CL in this sector is notable, highlighting this trend. Analytically, through the EPR and LRR methods, there is a significant erosion vector in this segment. Quantified data reveal an average variability of -2.38 m/year and -2.13 m/year, respectively, for the two methods. The maximum

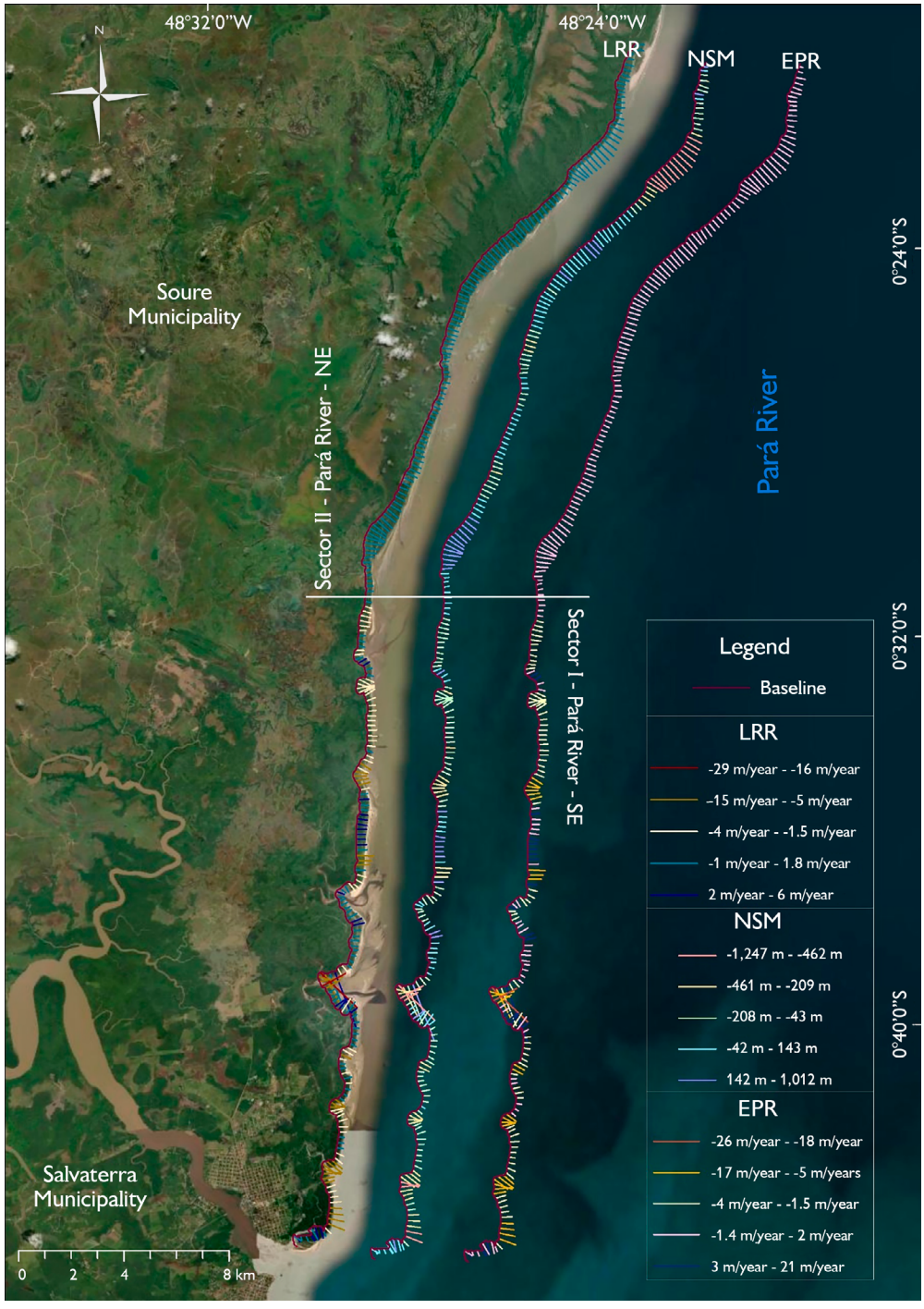

Figure 4. Map of End Point Rate (EPR) and Linear Regression Rate (LRR) at the western edge of the Pará River estuary, municipality of Soure, Marajó Island, Pará, 2020. Source: Author (2024).

erosion retreat is -26.6 m/year (transect 586), averaging -3.53 m/year among negative EPR values. In contrast, LRR exhibits -29.41 m/year (transect 586), averaging -3.94 m/year among erosive values (Figures 4, 5B and 5C, Table 4).

Accretion values the CL show a maximum positive rate of 21.59 m/year (transect 583), with an average of 3.82 m/year, and 5.83 m/year (transect 583), with an average variability of 2.34 m/year, for the underlying methods highlighted (Figure 4).

SECTOR II – PARÁ RIVER – NE

Sector II (~23 km) comprises 122 transects (375-496), where the rates from statistical models reflect a dynamic characterized by stabilization tendencies with erosive trends. It is evident that 76 transects (62%) exhibit stabilization tendencies, while 46 transects (38%) show erosive tendencies. However, erosive rates surpass those of accretion transects, resulting in a coastline variation of 0.2 m/year (Figure 4).

Table 3. Coastline change rates from Zone-I to Zone-II (1972–2020). Source: Author (2024).

Descriptive statistics	Sector I	Sector II	Total
Transect ID	497-656	375-496	375-656
Total number of transects	160	122	282
Coastline length (km)	27	23	50
Total number of transects where erosion was recorded	114	46	160
Total number of transects where accretion was recorded	46	76	122
Total number of transects where statistical uncertainty ($R > 0.5$) was recorded	87	26	113
Total number of transects where statistical uncertainty ($R < 0.5$) was recorded	73	96	169
% of total number of transects where erosion was recorded	71	38	57
% of total number of transects where accretion was recorded	29	62	43
% of total number of transects where statistical uncertainty ($R^2 > 0.5$) was recorded	54	21	40
% of total number of transects where statistical uncertainty ($R^2 < 0.5$) was recorded	46	79	60
Mean coastline change (m/year)	-2.1	0.2	-0.95
Maximum positive coastline change (m/year)	5.8	10.7	10.7
Maximum negative coastline change (m/year)	-29.4	-12.44	-29.4
Average accretion rate (m/year)	2.3	3.2	2.75
Average erosion rate (m/year)	-3.9	-4.8	4.35

Table 4. CL change rates for sectors I and II calculated using NSM (m), EPR, and LRR (m/year) methods between 1972–2020. Source: Author (2024).

Sectors	I			II		
Estatistics	NSM (m)	EPR (m/year)	LRR (m/year)	NSM (m)	EPR (m/year)	LRR (m/year)
Maximum negative rate	-1,247.46	-26.6	-29.41	-635.72	-13.55	-12.44
Maximum positive rate	1,012.72	21.59	5.83	490.81	10.46	10.68
Mean of negative rates	-193.5	-3.53	-3.94	-200.25	-4.3	-4.82
Mean of positive rates	110.07	3.82	2.34	119.75	2.55	3.23
Averages	-113.81	-2.38	-2.13	-51.54	-1.09	0.19

Statistical uncertainties with $R^2 > 0.5$ correspond to 26 transects, whereas 96 transects have $R^2 < 0.5$, representing 21% and 79%, respectively. These uncertainties indicate a trend towards stability or potential erosion over time (Table 3).

Net shoreline movement (NSM) rates show a trend towards stabilization despite sediment input, with an average of -51.54 m considering all negative and positive rates. The maximum erosion/recession rate is -635.72 m (transect 392), with an average rate of -200.25 m. In contrast, the maximum positive rate reaches 490.81 m (transect 486), with an average rate of 119.75 m (Figures 4 and 6A, Table 4).

EPR and LRR methods indicate rates skewed towards erosive processes. Specifically, average variabilities are -1.09 m/year and 0.19 m/year, respectively. The maximum erosive rate reaches -13.55 m/year (transect 392) with an average of -4.30 m/year for EPR, and -12.44 m/year (transect 392) with an average of -4.82 m/year for LRR. Meanwhile, the maximum positive rates are 10.46 m/year (transect 486) with an average of 2.55 m/year, and 10.68 m/year (transect 486) with an average variability of 3.23 m/year, as observed through the methods applied (Figures 4, 6B and 6C, Table 4).

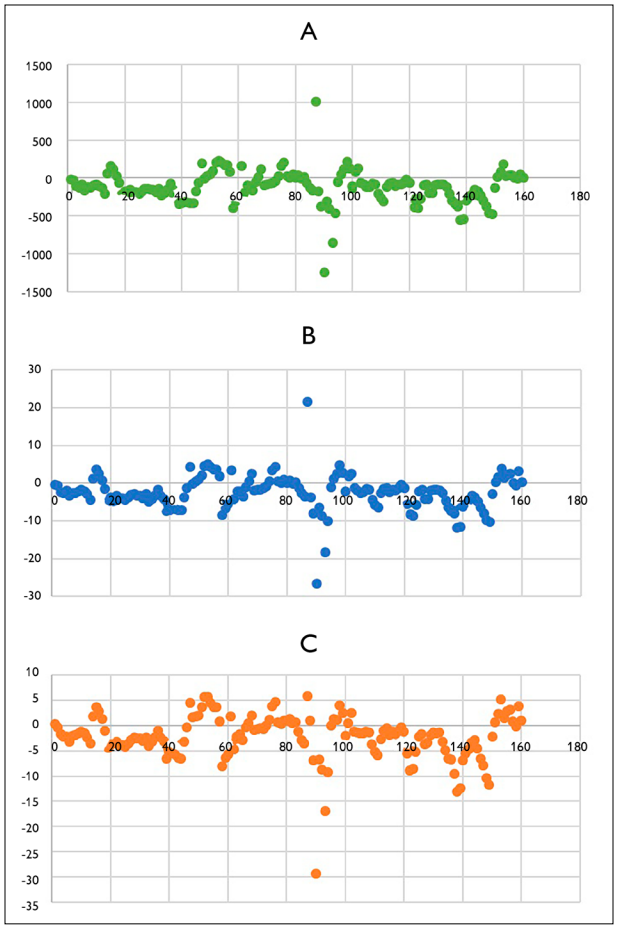

Figure 5. Net Shoreline Movement (NSM-A), End Point Rate (EPR-B), and Linear Regression Rate (LRR-C) in Sector I of Soure municipality, Marajó Island, Pará. Source: Author (2024).

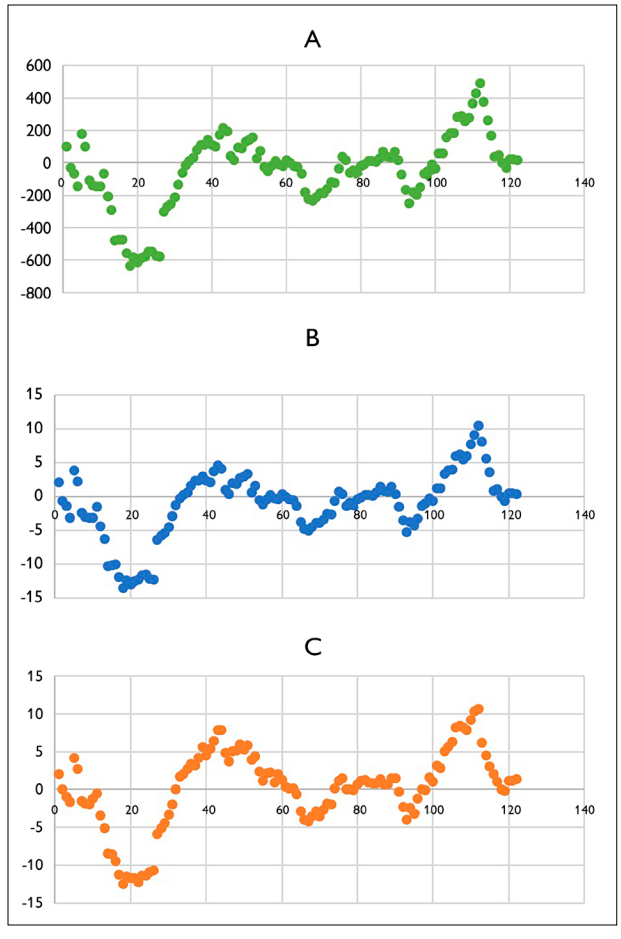

Figure 6. Net Shoreline Movement (NSM-A), End Point Rate (EPR-B), and Linear Regression Rate (LRR-C) in Sector II of Soure municipality, Marajó Island, Pará. Source: Author (2024).

DISCUSSION

The scenario of sectors I and II, where both are influenced by the dynamics of the waters from the Pará River estuary, characterized by a predominance of semidiurnal macrotides with secondary importance of diurnal oscillations (both astronomically driven), is generated due to the nonlinear interaction among the main harmonic constituents, especially the M4 (Prestes et al., 2020). According to the same authors, tidal currents (2 m^3s^{-1}) associated with river discharge (20,946 m^3s^{-1}) favor erosive effects, as the energy distribution associated with CL on the left bank of the Pará River acts as a remover of sediment particles, favoring accretion on the right bank of this river. On the eastern bank, the structure corresponding to the Barreiras sediments is represented by sandstones and claystones followed by Post-Barreiras sediments (Rossetti et al., 2008a, 2008b), which identifies the accretive content and type of deposits in this spatial scenario.

In sector II, the average LC variation is 0.2 m/year, and the average among all NSM rates, negative and positive, corresponds to -51.54 m. It exhibits a maximum erosion rate of -635.72 ± 200.25 m, whereas the maximum positive rate is 490.81 m ± 119.75 m. The EPR and LRR average -1.09 m/year and 0.19 m/year, respectively, indicating a trend towards erosion.

Sector I, on the other hand, is typically erosive with an average LC retreat rate of -2.1 m/year. The NSM averages -113.81 m, with a maximum erosive rate of -1,247.46 m ± 193.5 m, and a positive scenario of 1,012.72 m ± 110.07 m. The EPR averages -2.38 m/year, and LRR averages -2.13 m/year.

The western bank exhibits a tendency towards erosion, considering the erosive effects in the South Channel of the Amazon River, where strong tidal currents are linked to tides (maximum of 4.2 m at spring tide, with a variation of 0.5-1.2 m between neap tide or quadrature) (Rosário, 2016). This is due to the Pará River estuary experiencing intense riverine input combined with the co-oscillation of astronomical tides, resulting in a distinct hydrodynamic pattern and complex mixing process. Sediments on this bank consist mainly of medium to fine sand (Corrêa, 2006). Another factor to consider is that this bank is more exposed to winds entering the South Channel at speeds ranging from 2 m/s to 7 m/s (INMET, n.d.), which contributes to increased erosion.

The accretion of the CL in this geographical area is related to the distribution pattern of suspended material, where it reaches a maximum of 0.385 $m^{-1}s^{-1}$ and a minimum of 0.112 $m^{-1}s^{-1}$ without current inversion (Carneiro et al., 2020) (Figure 7). Thus, the data obtained by Carneiro et al. (2020) estimated that the export of suspended solids (TSSL) reached a maximum value of 0.9229 kg $m^{-1}s^{-1}$ in the dry season and 0.6650 kg $m^{-1}s^{-1}$ in the rainy period. This condition is also influenced by the Amazon River plume, which deposits sediments in the vicinity of the Pará River estuary margins. Furthermore, the penetrating tides are important for regulating the dynamics of suspended solids in estuaries and, particularly, in the Pará River estuary, where the river discharge is 20,946 m^3s^{-1} (Prestes et al., 2020), imparting to this region a significant kinetic energy perpendicular to the CL, where the net input of the continental regime reacts and integrates directly with the barotropic flow generated by tidal currents.

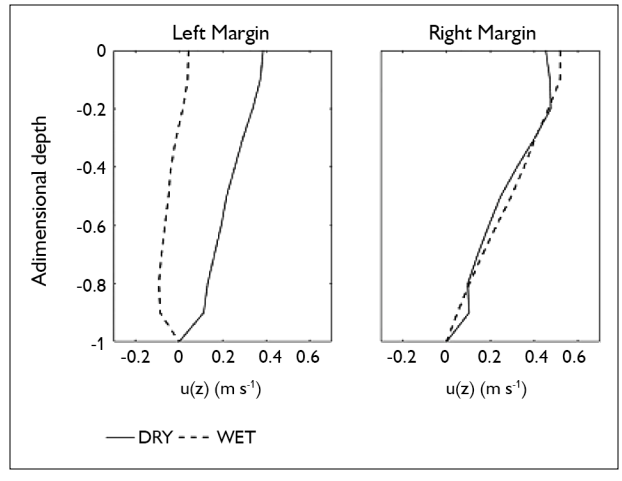

Figure 7. Vertical residual profiles of the u-velocity component for the dry season (solid line) and rainy season (dashed line) on both banks of the Pará River estuary. Source: Prestes et al. (2020).

Thus, some researchers reached similar results (Baig et al., 2020; Benkhattab et al., 2020; Galvez et al., 2020; Kabir et al., 2020; Mishra et al., 2020; Muskananfola et al., 2020; Warnasuriya et al., 2020; C. A. G. Santos et al., 2021b). Santos et al. (2021), on the beaches of Bessa and Intermares Campina, using the EPR method, reported values of -1.20 m/year and 0.94 m/year for the maximum and minimum rates, respectively. Using the LRR method, the minimum and maximum rates of CL change were -0.90 m/year and 1.22 m/year, which indicates a process similar to the dynamics occurring in sector II.

In contrast, for Ponta do Seixas beach, these authors reported rates for the EPR (-0.39 m/year) were higher than the LRR values (-0.32 m/year), indicating an amplitude of erosive character, similar to sector I, located southeast of Soure.

The rainy and dry seasons influenced by the ITCZ (Intertropical Convergence Zone) and the El Niño (EN) and La Niña phenomena (Figure 8) are also relevant to the estuary's flow. In an average analysis period, possible changes related to extreme events are considered in addition to seasonal changes. All factors that influence river discharge, currents, and tides, whether over a long or short period, are relevant to coastal changes.

The CL's of the beaches that are the subjects of this manuscript were influenced by these factors. In Figure 8, it is possible to observe the temporal alternations of extreme events related to EN and LN. In the context of EN, it influenced sediment input, especially during its 'very strong' characteristic phases occurring in 1990-1993, 1997-1998, and 2015-2016. This extreme phenomenon affects the climate of the Amazon, characterized by a significant reduction in rainfall, which decreases the flow of the Pará River and, consequently, fluvial erosion. Thus, opposite extreme conditions can occur, focusing on the transition to LN. This extreme, unlike EN, causes a substantial increase in sediment input due to the association with the ITCZ and the displacement of the Walker cell (INMET, 2021). These extreme events, combined with anthropogenic and hydrographic/oceanographic factors, were fundamental in the erosive reworking and accretion in the study area, especially during the analysis period of the CL's.

FINAL CONSIDERATIONS

The methodology employed, using semi-automatic methods derived from the spatial analysis of orbital images acquired by remote sensors (Landsat) and utilizing DSAS v5, has enabled significant scientific advancements for the Amazon region and holds global importance. Throughout the manuscript, geoprocessing tools and techniques are used that can be replicated in other CZ, systematically contributing technical, theoretical, and methodological support for policy makers in management.

The challenges of implementing this set of techniques are numerous. However, the acquisition of a more accurate temporal and spatial dataset, with less cloud cover, stands out as nearly unfeasible due to the

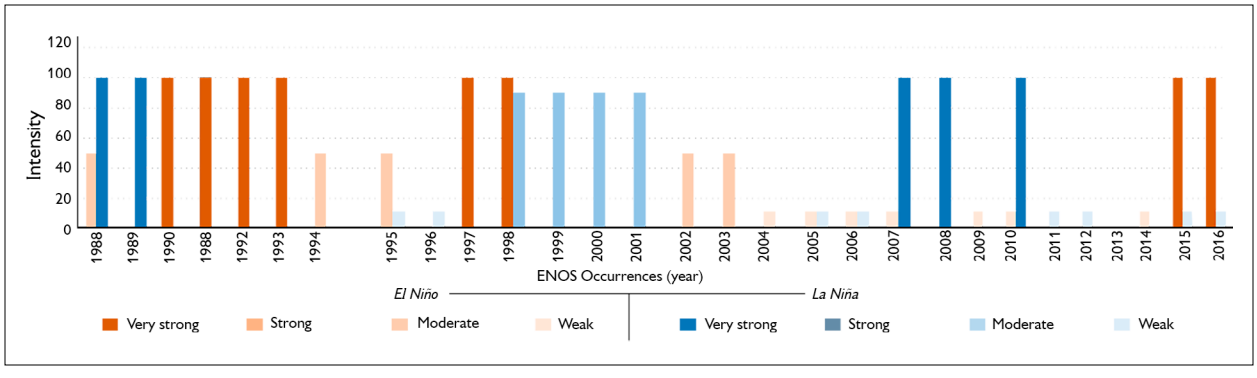

Figure 8. Historical occurrences of El Niño and La Niña. Source: CPTEC (2019).

study area being located in the ITCZ. An alternative to address this issue is the use of active sensors (synthetic aperture radar) and/or photogrammetry from unmanned aerial vehicles (UAVs), integrating them with the data available and utilized in this study and others under the perspective of this manuscript.

The results made it possible to identify that each area of the sector is marked by different dynamics according to its exposure to coastal factors. Thus, the results achieved are relevant, as the analysis can be used by public administrators considering that the sectors of the eastern margin of Soure municipality do not exhibit uniform dynamics throughout their extent.

Despite the significant progress made through this work, more in-depth analyses of the processes controlling the retreat and accretion of the CL in this geographical area are still necessary. The information obtained in this study summarizes only some parameters (statistical rates and CL mobility) of the dynamics, which are suitable for case studies (in situ). A greater acquisition of recent oceanographic and geological data, as well as a comprehensive set of orbital data, is essential because this region is still underrepresented in integrated studies regarding these scientific areas. This will allow for the evaluation of probable predictive scenarios for the evolution of the CL.

Finally, the analysis conducted in this region, integrated with the processes affecting the CL of Marajó Island (where the study area is located), provides a fragmentary understanding of a more complex dynamic. However, it can contribute as a basis for future research on coastal dynamics in other regions, adding informational mechanisms that serve as a predictive model for environmental changes on a large temporal and spatial scale using remote sensing and geoprocessing techniques.

REFERENCES

Agência Nacional de Águas e Saneamento Básico (ANA). (2021). *Base de Bacias Hidrográficas do Brasil – BHB250* [conjunto de dados geoespaciais]. https://metadados.snirh.gov.br/geonetwork/srv/api/records/3d87216f-e45e-41d8-9837-074c1608fb1e

Ahmed, N., Howlader, N., Hoque, M. A., & Pradhan, B. (2021). Coastal erosion vulnerability assessment along the eastern coast of Bangladesh using geospatial techniques. *Ocean & Coastal Management*, *199*, 105408. https://doi.org/10.1016/j.ocecoaman.2020.105408

Al-Hatrushi, S. M. (2013). Monitoring of the shoreline change using remote sensing and GIS: a case study of Al Hawasnah tidal inlet, Al Batinah coast, Sultanate of Oman. *Arabian Journal of Geosciences*, *6*(5), 1479–1484. https://doi.org/10.1007/s12517-011-0424-2

Alesheikh, A. A., Ghorbanali, A., & Nouri, N. (2007). Coastline change detection using remote sensing. *International Journal of Environmental Science & Technology*, *4*(1), 61–66. https://doi.org/10.1007/BF03325962

Allan, J. C., Komar, P. D., & Priest, G. R. (2003). Shoreline variability on the high-energy Oregon Coast and its usefulness in erosion-hazard assessments. *Journal of Coastal Research*, *38*, 83–105. http://jstor.org/stable/25736601

Almonacid-Caballer, J., Sánchez-García, E., Pardo-Pascual, J. E., Balaguer-Beser, A. A., & Palomar-Vázquez, J. (2016). Evaluation of annual mean shoreline position deduced from Landsat imagery as a mid-term coastal evolution indicator. *Marine Geology*, *372*, 79–88. https://doi.org/10.1016/j.margeo.2015.12.015

Aquino da Silva, A. G., Silva, A. G. A., Stattegger, K., Vital, H., & Schwarzer, K. (2019). Coastline change and offshore suspended sediment dynamics in a naturally developing delta (Parnaíba Delta, NE Brazil). *Marine Geology*, *410*, 1–15. https://doi.org/10.1016/j.margeo.2018.12.013

Ataol, M., Kale, M. M., & Tekkanat, I. S. (2019). Assessment of the changes in shoreline using digital shoreline analysis system: a case study of Kizilirmak Delta in northern Turkey from 1951 to 2017. *Environmental Earth Sciences*, *78*, 579. https://doi.org/10.1007/s12665-019-8591-7

Baía, L. B., Ranieri, L. A., & Rosário, R. P. (2021). Análise multitemporal da variação da linha de costa em praias estuarinas do Nordeste do Pará. *Geociências*, *40*(1), 231–244. https://doi.org/10.5016/geociencias.v40i1.13470

Baig, M. R. I., Ahmad, I. A., Shahfahad, Tayyab, M., & Rahman, A. (2020). Analysis of shoreline changes in Vishakhapatnam coastal tract of Andhra Pradesh, India: an application of digital shoreline analysis system (DSAS). *Annals of GIS*, *26*(4), 361–376. https://doi.org/10.1080/19475683.2020.1815839

Baral, R., Pradhan, S., Samal, R. N., & Mishra, S. K. (2018). Shoreline Change Analysis at Chilika Lagoon Coast, India Using Digital Shoreline Analysis System. *Journal of the Indian Society of Remote Sensing*, *46*(10), 1637–1644. https://doi.org/10.1007/s12524-018-0818-7

Benkhattab, F. Z., Hakkou, M., Bagdanavičiūtė, I., El Mrini, A., Zagaoui, H., Rhinane, H., & Maanan, M. (2020). Spatial–temporal analysis of the shoreline change rate using automatic computation and geospatial tools along the Tetouan coast in Morocco. *Natural Hazards*, *104*(1), 519–536. https://doi.org/10.1007/s11069-020-04179-2

Bertacchini, E. (2010). Map updating and coastline control with very high resolution satellite images: application to Molise and Puglia coasts (Italy). *Italian Journal of Remote Sensing*, *42*(2), 103–115.

Bheeroo, R. A., Chandrasekar, N., Kaliraj, S., & Magesh, N. S. (2016). Shoreline change rate and erosion risk assessment along the Trou Aux Biches–Mont Choisy beach on the northwest coast of Mauritius using GIS-DSAS technique. *Environmental Earth Sciences*, *75*(5), 444. https://doi.org/10.1007/s12665-016-5311-4

Boye, C. B., Appeaning Addo, K., Wiafe, G., & Dzigbodi-Adjimah, K. (2018). Spatio-temporal analyses of shoreline change in the Western Region of Ghana. *Journal of Coastal Conservation*, *22*(4), 769–776. https://doi.org/10.1007/s11852-018-0607-z

Carneiro, A. G., Prestes, Y. O., & Rollnic, M. (2020). Estimates of suspended solid transport in the pará river estuary. *Ocean and Coastal Research*, *68*, e20281. https://doi.org/10.1590/S2675-28242020068281

Carvalho, B. C., Dalbosco, A. L. P., & Guerra, J. V. (2020). Shoreline position change and the relationship to annual and interannual meteo-oceanographic conditions in Southeastern Brazil. *Estuarine, Coastal and Shelf Science*, *235*, 106582. https://doi.org/10.1016/j.ecss.2020.106582

Centro de Previsão de Tempo e Estudos Climáticos (CPTEC). (2019). *Monitoramento do El Niño durante DJF-2019*. INPE. http://enos.cptec.inpe.br/

Chenthamil Selvan, S., Kankara, R. S., Markose, V. J., Rajan, B., & Prabhu, K. (2016). Shoreline change and impacts of coastal protection structures on Puducherry, SE coast of India. *Natural Hazards*, *83*(1), 293–308. https://doi.org/10.1007/s11069-016-2332-y

Conti, L. A., & Rodrigues, M. (2011). Variação da linha de costa na região da Ilha dos Guarás – PA através de análise de série temporal de imagens de satélites. *Revista Brasileira de Geografia Física*, *4*(5), 922–937. https://doi.org/10.26848/rbgf.v4i5.232745

Corrêa, I. C. S. (2006). Aplicação do diagrama de Pejrup na interpretação da sedimentação e da dinâmica do estuário da baía de Marajó-PA. *Pesquisa em Geociências*, *32*(2), 109–118. https://doi.org/10.22456/1807-9806.19551

Ding, X., Shan, X., Chen, Y., Jin, X., & Muhammed, F. R. (2019). Dynamics of shoreline and land reclamation from 1985 to 2015 in the Bohai Sea, China. *Journal of Geographical Sciences*, *29*(12), 2031–2046. https://doi.org/10.1007/s11442-019-1703-1

Dolan, R., Fenster, M. S., & Holme, S. J. (1991). Temporal analysis of shoreline recession and accretion. *Journal of Coastal Research*, *7*(3), 22. https://journals.flvc.org/jcr/article/view/78527

Duarte, C. R., Miranda, F. P., Landau, L., Souto, M. V. S., Sabadia, J. A. B., Silva Neto, C. Â., Rodrigues, L. I. C., & Damasceno, A. M. (2018). Short-time analysis of shoreline based on RapidEye satellite images in the terminal area of Pecém Port, Ceará, Brazil. *International Journal of Remote Sensing*, *39*(13), 4376–4389. https://repositorio.ufc.br/handle/riufc/64578

El-Robrini, M., Ranieiri, L. A., Silva, P. V. M., Guerreiro, J. S., Alves, M. A. M. S., Oliveira, R. R. S., Amora, P. B. C., El-Robrini, M. H. S., Fenzl, N., & Farias, D. R. (2018). Pará. In D. Muehe (Ed.), *Panorama da erosão costeira no Brasil* (p. 759). Ministério do Meio Ambiente, Secretaria de Recursos Hídricos e Qualidade Ambiental, Departamento de Gestão Ambiental Rural.

Esmail, M., Mahmod, W. E., & Fath, H. (2019). Assessment and prediction of shoreline change using multi-temporal satellite images and statistics: Case study of Damietta coast, Egypt. *Applied Ocean Research*, *82*, 274–282. https://doi.org/10.1016/j.apor.2018.11.009

Farias, E. G. G., & Maia, L. P. (2010). Uso de técnicas de geoprocessamento para a análise da evolução da linha de costa em ambientes litorâneos do estado do Ceará, Brasil. *Revista de Gestão Costeira Integrada*, *10*(4), 521–544. https://www.aprh.pt/rgci/pdf/rgci-224_Farias.pdf

França, C. F. (2003). *Morfologia e mudanças costeiras na margem leste de Marajó (PA)* [Tese de doutorado, Universidade Federal do Pará]. https://repositorio.ufpa.br/items/e07139d1-561c-4dba-9a82-ace57a2ad1c7

França, C. F., & Souza Filho, P. W. M. E. (2003). Análise das mudanças morfológicas costeiras de médio período na margem leste da ilha de Marajó (PA) em imagem Landsat. *Revista Brasileira de Geociências*, *33*(2), 127–136. https://ppegeo.igc.usp.br/portal/index.php/rbg/analise-das-mudancas-morfologicas-costeiras-de-medio-periodo-na-margem-leste-da-ilha-de-marajo-pa-em-imagem-landsat/

Galvez, D. S., Papenmeier, S., Hass, H. C., Bartholomae, A., Fofonova, V., & Wiltshire, K. H. (2020). Detecting shifts of submarine sediment boundaries using side-scan mosaics and GIS analyses. *Marine Geology*, *430*, 106343. https://doi.org/10.1016/j.margeo.2020.106343

Genz, A. S., Fletcher, C. H., Dunn, R. A., Frazer, L. N., & Rooney, J. J. (2007). The predictive accuracy of shoreline change rate methods and alongshore beach variation on Maui, Hawaii. *Journal of Coastal Research*, (231), 87–105. https://doi.org/10.2112/05-0521.1

Himmelstoss, E. A., Henderson, R. E., Farris, A. S., Kratzmann, M. G., Bartlett, M. K., Ergul, A., McAndrews, J., Cibaj, R., Zichichi, J. L., & Thieler, E. R. (2018). *Digital Shoreline Analysis System (versão 5.0). Um ArcGIS© extensão para o cálculo alteração na linha costeira: lançamento do software U.S*. https://code.usgs.gov/cch/dsas

Honeycutt, M. G., Crowell, M., & Douglas, B. C. (2001). Shoreline-Position Forecasting: Impact of Storms, Rate-Calculation Methodologies, and Temporal Scales. *Journal of Coastal Research*, *17*(3), 721–730. https://journals.flvc.org/jcr/article/view/81484

Instituto Brasileiro de Geografia e Estatística (IBGE). (2021). *Base cartográfica contínua do Brasil (BC250)* [conjunto de dados geoespaciais]. https://www.ibge.gov.br/geociencias/cartas-e-mapas/bases-cartograficas-continuas.html

Instituto Nacional de Meteorologia (INMET). (2021). *Normais climatológicas (1961/2019)*. https://portal.inmet.gov.br/servicos/normais-climatologicas

Instituto Nacional de Meteorologia (INMET). (n.d.). https://portal.inmet.gov.br/

Jana, A., Biswas, A., Maiti, S., & Bhattacharya, A. K. (2014). Shoreline changes in response to sea level rise along Digha Coast, Eastern India: an analytical approach of remote sensing, GIS and statistical techniques. *Journal of Coastal Conservation*, *18*(3), 145–155. https://doi.org/10.1007/s11852-013-0297-5

Kabir, M. A., Salauddin, M., Hossain, K. T., Tanim, I. A., Saddam, M. M. H., & Ahmad, A. U. (2020). Assessing the shoreline dynamics of Hatiya Island of Meghna estuary in Bangladesh using multiband satellite imageries and hydro-meteorological data. *Regional Studies in Marine Science*, *35*, 101167. https://doi.org/10.1016/j.rsma.2020.101167

Kaliraj, S., Chandrasekar, N., & Magesh, N. S. (2015). Evaluation of coastal erosion and accretion processes along the southwest coast of Kanyakumari, Tamil Nadu using geospatial techniques. *Arabian Journal of Geosciences*, *8*(1), 239–253. https://doi.org/10.1007/s12517-013-1216-7

Kannan, R., Anand, K. V., Sundar, V., Sannasiraj, S. A., & Rangarao, V. (2014). Shoreline changes along the Northern coast of Chennai port, from field measurements. *ISH Journal of Hydraulic Engineering*, *20*(1), 24–31. https://doi.org/10.1080/09715010.2013.821789

Lacerda, M., Vasquez, M., & Rosa-Costa, L. T. (2008). *Geologia e recursos minerais do Estado do Pará: Sistema de Informações Geográficas (SIG): Texto explicativo dos mapas geológico, tectônico e de recursos minerais do Estado do Pará (Escala 1:1.000.000)*. CPRM.

Li, X., Zhou, Y., Tian, B., Kuang, R., & Wang, L. (2015). GIS-based methodology for erosion risk assessment of the muddy coast in the Yangtze Delta. *Ocean & Coastal Management*, *108*, 97–108. https://doi.org/10.1016/j.ocecoaman.2014.09.028

Lima, A. M. M., Oliveira, L. L., Fontinhas, R. L., & Lima, R. J. S. (2005). Ilha do Marajó: revisão histórica, hidroclimatológica, bacias hidrográficas e proposta de gestão. *Holos Environment*, *5*(1), 65. https://doi.org/10.14295/holos.v5i1.331

Lima, L. T., Fernández-Fernández, S., Espinoza, J. M. A., Albuquerque, M. G., & Bernardes, C. (2021). End point rate tool for QGIS (EPR4Q): Validation using DSAS and AMBUR. *International Journal of Geo-Information*, *10*(3), 162. https://doi.org/10.3390/ijgi10030162

Luijendijk, A., Hagenaars, G., Ranasinghe, R., Baart, F., Donchyts, G., & Aarninkhof, S. (2018). The state of the world's beaches. *Scientific Reports*, *8*(1), 6641. https://doi.org/10.1038/s41598-018-24630-6

Mahapatra, M., Ratheesh, R., & Rajawat, A. S. (2014a). Shoreline change analysis along the Coast of South Gujarat, India, using digital shoreline analysis system. *Journal of the Indian Society of Remote Sensing*, *42*(4), 869–876. https://doi.org/10.1007/s12524-013-0334-8

Mahapatra, M., Ratheesh, R., & Rajawat, A. S. (2014b). Shoreline change analysis along the coast of South Gujarat, India, using digital shoreline analysis system. *Journal of the Indian Society of Remote Sensing*, *42*(4), 869–876. https://doi.org/10.1007/s12524-013-0334-8

Maiti, S., & Bhattacharya, A. K. (2009). Shoreline change analysis and its application to prediction: A remote sensing and statistics based approach. *Marine Geology*, *257*(1–4), 11–23. https://doi.org/10.1016/j.margeo.2008.10.006

Marinha do Brasil. (n.d.). *Tábuas de maré*. Diretoria de Hidrografia e Navegação. https://www.marinha.mil.br/chm/tabuas-de-mare

Mcfadden, L., Nicholls, R., Vafeidis, A., & Tol, R. (2007). A methodology for modeling coastal space for global assessment. *Journal of Coastal Research*, *23*(4), 911–920. https://doi.org/10.2112/04-0365.1

Melo, L. B., & Simões, P. (2016) *Ação emergencial para delimitação de áreas em alto e muito alto risco a enchentes e movimentos de massa: Soure - Ilha do Marajó, Pará*. CPRM. https://rigeo.sgb.gov.br/handle/doc/18370

Mentaschi, L., Vousdoukas, M. I., Pekel, J.-F., Voukouvalas, E., & Feyen, L. (2018). Global long-term observations of coastal erosion and accretion. *Scientific Reports*, *8*(1), 12876. https://doi.org/10.1038/s41598-018-30904-w

Ministério do Meio Ambiente (MMA). (2018). *Panorama da erosão costeira no Brasil*. MMA. https://www.bivica.org/file/view/id/5975

Mishra, M., Chand, P., Pattnaik, N., Kattel, D. B., Panda, G. K., Mohanti, M., Baruah, U. D., Chandniha, S. K., Achary, S., & Mohanty, T. (2019). Response of long- to short-term changes of the Puri coastline of Odisha (India) to natural and anthropogenic factors: a remote sensing and statistical assessment. *Environmental Earth Sciences*, *78*(11), 338. https://doi.org/10.1007/s12665-019-8336-7

Mishra, M., Sudarsan, D., Kar, D., Naik, A. K., Das, P. P., Santos, C. A. G., & Silva, R. M. (2020). The development and research trend of using dsas tool for shoreline change analysis: A scientometric analysis. *Journal of Urban and Environmental Engineering*, *14*(1), 69-77. https://doi.org/10.4090/juee.2020.v14n1.69-77

Mishra, M., Acharyya, T., Chand, P., Santos, C. A. G., Kar, D., Das, P. P., Pattnaik, N., Silva, R. M. da, & Nascimento, T. V. M. (2022). Analyzing shoreline dynamicity and the associated socioecological risk along the Southern Odisha Coast of India using remote sensing-based and statistical approaches. *Geocarto International*, *37*(14), 3991–4027. https://doi.org/10.1080/10106049.2021.1882005

Misra, A., & Balaji, R. (2015). A study on the shoreline changes and LAND-use/ land-cover along the South Gujarat Coastline. *Procedia Engineering*, *116*(1), 381–389. https://doi.org/10.1016/j.proeng.2015.08.311

Muskananfola, M. R., Supriharyono, Febrianto, S. (2020). Spatio-temporal analysis of shoreline change along the coast of Sayung Demak, Indonesia using Digital Shoreline Analysis System. *Regional Studies in Marine Science*, *34*, 101060. https://doi.org/10.1016/j.rsma.2020.101060

Nascimento, L. (2012). *Comportamento da linha de costa nos últimos 50 anos e o risco de prejuízos econômicos na face oceânica da ilha de Itaparica – Bahia* [Tese de doutorado, Universidade Federal da Bahia]. https://repositorio.ufba.br/handle/ri/21498

Nassar, K., Mahmod, W. E., Fath, H., Masria, A., Nadaoka, K., & Negm, A. (2019). Shoreline change detection using DSAS technique: Case of North Sinai coast, Egypt. *Marine Georesources & Geotechnology*, *37*(1), 81–95. https://doi.org/10.1080/1064119X.2018.1448912

Orlando, L., Ortega, L., & Defeo, O. (2019). Multi-decadal variability in sandy beach area and the role of climate forcing. *Estuarine, Coastal and Shelf Science*, *218*, 197–203. https://doi.org/10.1016/j.ecss.2018.12.015

Pará. (2020, 25 maio). Lei ordinária nº 9.064, de 25 de maio de 2020. Institui a Política Estadual de Gerenciamento Costeiro (PEGC/PA). *Diário Oficial do Estado do Pará*. https://www.semas.pa.gov.br/legislacao/normas/view/6556

Pessoa, R. M. C., Jiménez, J. A., Costa, R. M., & Pereira, L. C. C. (2019). Federal conservation units in the Brazilian amazon coastal zone: An adequate approach to control recreational activities? *Ocean & Coastal Management*, *178*, 104856. https://doi.org/10.1016/j.ocecoaman.2019.104856

Prestes, Y. O., Rollnic, M., Sousa, M., & Rosario, R. P. (2014). Volume transport in the tidal limit of the Pará River, Brazil. In *Proceedings of the 17th Physics of Estuaries and Coastal Seas Conference (PECS)*, Porto de Galinhas, PE, Brasil.

Prestes, Y. (2016). *Interações físicas entre o estuário do rio Pará e a plataforma continental no norte do Brasil* [Dissertação de mestrado, Universidade Federal de Pernambuco].

Prestes, Y. O., Silva, A. C., Rollnic, M., & Rosário, R. P. (2017). The M2 and M4 tides in the Pará River Estuary. *Tropical Oceanography*, *45*(1), 26–37. https://doi.org/10.5914/tropocean.v45i1.15198

Prestes, Y. O., Borba, T. A. C., Silva, A. C., & Rollnic, M. (2020). A discharge stationary model for the Pará-Amazon estuarine system. *Journal of Hydrology: Regional Studies*, *28*, 100668. https://doi.org/10.1016/j.ejrh.2020.100668

Quadrado, G. P., Dillenburg, S. R., Goulart, E. S., & Barboza, E. G. (2021). Historical and geological assessment of shoreline changes at an urbanized embayed sandy system in Garopaba, Southern Brazil. *Regional Studies in Marine Science*, *42*, 101622. https://doi.org/10.1016/j.rsma.2021.101622

Ranieri, L. A., & El-Robrini, M. (2015). Evolution of the Salinópolis shoreline, Northeastern of Pará, Brazil. *Pesquisas em Geociencias*, *42*(3), 207–226. https://seer.ufrgs.br/index.php/PesquisasemGeociencias/article/view/78121/44732

Rodrigues, S. W. P., & Souza Filho, P. W. M. E. (2011). Análise da variação da linha de costa a noroeste do Estado do Pará (Baía de Curuçá) através das imagens Landsat TM e ETM$^+$ e CBERS 2B. *Anais do XV Simpósio Brasileiro de Sensoriamento Remoto (SBSR)*. INPE. http://marte.dpi.inpe.br/col/dpi.inpe.br/marte/2011/07.25.14.31/doc/p1525.pdf

Rosário, R. P. (2016). *Análise de processos oceanográficos no estuário do rio Pará* [Tese de doutorado, Universidade Federal do Pará]. http://repositorio.ufpa.br/jspui/handle/2011/8876

Rosário, R. P., Borba, T. A. C., Santos, A. S., & Rollnic, M. (2016). Variability of Salinity in Pará River Estuary: 2D Analysis with Flexible Mesh Model. *Journal of Coastal Research*, *75*(sp1), 128–132. https://doi.org/10.2112/SI75-026.1

Rossetti, D. F., Góes, A. M., Valeriano, M. M., & Miranda, M. C. C. (2008a). Quaternary tectonics in a passive margin: Marajó Island, northern Brazil. *Journal of Quaternary Science*, *23*(2), 121–135. https://doi.org/10.1002/jqs.1132

Rossetti, D. F., Valeriano, M. M., Góes, A. M., & Thales, M. (2008b). Palaeodrainage on Marajó Island, northern Brazil, in relation to Holocene relative sea-level dynamics. *The Holocene*, *18*(6), 923–934. https://doi.org/10.1177/0959683608091798

Santos, C. A. (2017). *Sensoriamento remoto aplicado ao estudo da evolução espaço-temporal da dinâmica vegetal do manguezal em barra de Guaratiba - RJ* [Trabalho de conclusão de curso, Universidade Federal Fluminense]. https://app.uff.br/riuff/handle/1/3424

Santos, C. A. G., Nascimento, T. V. M., Mishra, M., & Silva, R. M. (2021a). Analysis of long- and short-term shoreline change dynamics: A study case of João Pessoa city in Brazil. *Science of the Total Environment*, *769*, 144889. https://doi.org/10.1016/j.scitotenv.2020.144889

Santos, C. A. G., Nascimento, T. V. M., Mishra, M., & Silva, R. M. (2021b). Analysis of long- and short-term shoreline change dynamics: A study case of João Pessoa city in Brazil. *Science of the Total Environment*, *769*, 144889. https://doi.org/10.1016/j.scitotenv.2020.144889

Silva, G. V., Muler, M., Prado, M. F. V., Short, A. D., Klein, A. H. F., & Toldo, E. E. (2016). Shoreline change analysis and insight into the sediment transport path along Santa Catarina Island north shore, Brazil. *Journal of Coastal Research*, *32*(4), 863–874. https://doi.org/10.2112/JCOASTRES-D-15-00164.1

Souza Filho, P. W. M. (2005). Costa de manguezais de macromaré da Amazônia: cenários morfológicos, mapeamento e quantificação de áreas usando dados de sensores remotos. *Revista Brasileira de Geofísica*, *23*(4), 427–435. https://doi.org/10.1590/S0102-261X2005000400006

Stanchev, H., Stancheva, M., Young, R., & Palazov, A. (2018). Analysis of shoreline changes and cliff retreat to support Marine Spatial Planning in Shabla Municipality, Northeast Bulgaria. *Ocean & Coastal Management*, *156*, 127–140. https://doi.org/10.1016/j.ocecoaman.2017.06.011

Tran Thi, V., Tien Thi Xuan, A., Phan Nguyen, H., Dahdouh-Guebas, F., & Koedam, N. (2014). Application of remote sensing and GIS for detection of long-term mangrove shoreline changes in Mui Ca Mau, Vietnam. *Biogeosciences*, *11*(14), 3781–3795. https://doi.org/10.5194/bg-11-3781-2014

United States Geological Survey (USGS). (2018). *USGS EROS Archive—Landsat Collection*. Earth Resources Observation and Science (EROS) Center.

Wang, Y., Hou, X., Jia, M., Shi, P., & Yu, L. (2014). Remote detection of shoreline changes in eastern bank of Laizhou Bay, North China. *Journal of the Indian Society of Remote Sensing*, *42*(3), 621–631. https://doi.org/10.1007/s12524-014-0361-0

Warnasuriya, T. W. S., Kumara, M. P., Gunasekara, S. S., Gunaalan, K., & Jayathilaka, R. M. R. M. (2020). An improved method to detect shoreline changes in small-scale beaches using Google Earth Pro. *Marine Geodesy*, *43*(6), 541–572. https://doi.org/10.1080/01490419.2020.1822478

AUTHORS' CONTRIBUTION

R. A. A. Menezes contributed to conceptualization, data curation, investigation, methodology and writing (original draft, review and editing); D. K. M. Guimarães contributed to writing (review and editing); and M. El Robrini contributed to supervision and writing (review and editing).